# Strain-domain structure and stability diagrams for single-domain magnetic thin films

J. J. Wang, Jia-Mian Hu, Long-Qing Chen, and Ce-Wen Nan

# Strain-domain structure and stability diagrams for single-domain magnetic thin films

J. J. Wang,[1,a)] Jia-Mian Hu,[1,a),b)] Long-Qing Chen,[1,2] and Ce-Wen Nan[1,b)]

[1]*State Key Lab of New Ceramics and Fine Processing, School of Materials Science and Engineering, Tsinghua University, Beijing 100084, China*

[2]*Department of Materials Science and Engineering, The Pennsylvania State University, University Park, Pennsylvania 16802, USA*

Strain effects on domain structures and thermal stability in single-domain magnetic thin films were studied using thermodynamic analysis. The strain-domain structure and stability diagrams were established and compared to several existing experimental results. The structure diagram displays various stable single-domain states under in-plane normal and/or in-plane shear strains by minimizing the free energy density whereas the stability diagram takes into account possible thermal excitations and hence illustrate the *thermally* stable magnetic single-domain states. The results improve the understanding of strain-magnetization correlation in magnetic thin films and provide useful insight for the development of strain-engineered magnetic nanostructures with novel functionalities. © 2013 AIP Publishing LLC. [http://dx.doi.org/10.1063/1.4824165]

In magnetic thin films, strain can be effectively utilized to tune the magnetic domain structures and hence properties.[1–4] For example, the magnetic domain/magnetization can be switched between an in-plane and out-of-plane orientation under isotropic biaxial in-plane strains,[5] or rotate within the film plane under anisotropic biaxial in-plane strains.[6] Strain may arise from the intrinsic lattice/thermal mismatch[7] or from the grain boundaries during Volmer-Weber film growth.[8] Strain also may be obtained through external piezoelectric and ferroelastic actuations,[9] opening up an appealing route towards low-power magnetic and spin-tronic devices[10] based on electric-voltage manipulated magnetism. In this regard, it is critically important to understand the details of strain-magnetization correlation in magnetic thin films.

In the present work, we focus on single-domain magnetic thin films whose smaller size[11] would make it competitive in high-density nanodevice designs. The strain-stabilized domain states in such uniformly magnetized thin films are obtained via analytical calculations.[5,6,12] By incorporating influences of both in-plane normal and shear strains, we provide a full set of thermodynamic potential herein that can be applied to describe the strain-magnetization correlation in single-domain thin-film magnets with either cubic (pseudocubic) or hexagonal crystal symmetry. Typical single-domain structures under various strain conditions are acquired by minimizing the total free energy with respect to magnetization. The strain-domain structure and stability diagrams are established by further taking into account possible thermal excitations.

The Gibbs free energy density of a magnetic bulk crystal can be written as a function of a unit magnetization vector **m** and stress tensor **σ**,[13] i.e.,

$$g(\mathbf{m}, \boldsymbol{\sigma}) = K_{ij}m_im_j + K_{ijkl}m_im_jm_km_l + K_{ijklpq}m_im_jm_km_lm_pm_q$$
$$- \frac{1}{2}s_{ijkl}\sigma_{ij}\sigma_{kl} - \lambda_{ijkl}m_im_j\sigma_{kl} + \frac{1}{2}\mu_0M_S^2N_{ij}m_im_j,$$

(1)

where $K_{ij}$, $K_{ijkl}$, and $K_{ijklpq}$ denote the first-, second-, and third-order magnetocrystalline anisotropic energy coefficients, respectively; $s_{ijkl}$ is the elastic compliance tensor; $\lambda_{ijkl}$ is the first-order magnetostriction coefficient tensor; $N_{ij}$ is the demagnetization factor tensor; $\mu_0$ is the vacuum permeability; and $M_S$ is the saturation magnetization.

For a magnetic thin film constrained laterally by a stiff substrate, an out-of-plane stress-free boundary condition should be superimposed, i.e.,

$$\sigma_{\alpha\beta} = c_{\alpha\beta\gamma\omega}(\varepsilon_{\gamma\omega} - \lambda_{\alpha\beta\gamma\omega}m_\alpha m_\beta), \quad (\alpha, \beta, \gamma, \omega = 1, 2)$$
$$\sigma_{k3} = \sigma_{3k} = 0, \quad (k = 1, 2, 3),$$

(2)

where $c_{ijkl}$ is the elastic stiffness tensor with value $c_{ijkl} = s_{ijkl}^{-1}$. $\varepsilon_{\gamma\omega}$ is the in-plane strains including the normal strains ($\varepsilon_{11}$, $\varepsilon_{22}$) and the shear strain $\varepsilon_{12}$ ($=\varepsilon_{21}$).

By combining Eqs. (1) and (2), the free energy density $f(\mathbf{m}, \boldsymbol{\varepsilon})$ of a constrained magnetic thin film can be obtained via the Legendre transformation of $g(\mathbf{m}, \boldsymbol{\sigma})$, i.e.,

$$f(\mathbf{m}, \boldsymbol{\varepsilon}) = g(\mathbf{m}, \boldsymbol{\sigma}) + \sigma_{\alpha\beta}\varepsilon_{\alpha\beta}$$
$$= K_{ij}m_im_j + K_{ijkl}m_im_jm_km_l + K_{ijklpq}m_im_jm_km_lm_pm_q$$
$$+ \frac{1}{2}c_{\alpha\beta\gamma\omega}(\varepsilon_{\alpha\beta} - \lambda_{\alpha\beta\gamma\omega}m_\gamma m_\omega)(\varepsilon_{\gamma\omega} - \lambda_{\alpha\beta\gamma\omega}m_\alpha m_\beta)$$
$$+ \frac{1}{2}\mu_0M_S^2N_{ij}m_im_j,$$
$$(i, j, k, l, p, q = 1, 2, 3 \text{ and } \alpha, \beta, \gamma, \omega = 1, 2),$$

(3)

where summation convention is used for the elastic stiffness tensor. For a cubic (001)-oriented magnetic thin film, Eq. (3) can be reduced as

---

[a)]These authors contribute equally to this work.

[b)]Authors to whom correspondence should be addressed. Electronic addresses: hjm08@mails.tsinghua.edu.cn and cwnan@tsinghua.edu.cn.

**103**, 142413-1

$$f^{\text{cubic}}(\mathbf{m}, \boldsymbol{\varepsilon}) = K_1(m_1^2 m_2^2 + m_1^2 m_3^2 + m_2^2 m_3^2) + K_2 m_1^2 m_2^2 m_3^2$$

$$+ \frac{1}{2} c_{11} \left[ \left( \varepsilon_{11} - \frac{3}{2} \lambda_{100} \left( m_1^2 - \frac{1}{3} \right) \right)^2 + \left( \varepsilon_{22} - \frac{3}{2} \lambda_{100} \left( m_2^2 - \frac{1}{3} \right) \right)^2 \right]$$

$$+ c_{12} \left( \varepsilon_{11} - \frac{3}{2} \lambda_{100} \left( m_1^2 - \frac{1}{3} \right) \right) \left( \varepsilon_{22} - \frac{3}{2} \lambda_{100} \left( m_2^2 - \frac{1}{3} \right) \right)$$

$$+ 2 c_{44} \left( \varepsilon_{12} - \frac{3}{2} \lambda_{111} m_1 m_2 \right)^2 + \frac{1}{2} \mu_0 M_S^2 (N_{11} m_1^2 + N_{22} m_2^2 + N_{33} m_3^2), \tag{4}$$

while for a hexagonal (0001)-oriented magnetic thin film,

$$f^{\text{hex}}(\mathbf{m}, \boldsymbol{\varepsilon}) = K_1(m_1^2 + m_2^2) + K_2(m_1^2 + m_2^2)^2$$

$$+ \frac{1}{2} c_{11} \left[ \left( \varepsilon_{11} - (\lambda_A m_1^2 + \lambda_B m_2^2) \right)^2 + \left( \varepsilon_{22} - (\lambda_A m_2^2 + \lambda_B m_1^2) \right)^2 \right]$$

$$+ c_{12} \left( \varepsilon_{11} - (\lambda_A m_1^2 + \lambda_B m_2^2) \right) \left( \varepsilon_{22} - (\lambda_A m_2^2 + \lambda_B m_1^2) \right)$$

$$+ (c_{11} - c_{12}) \left( \varepsilon_{12} - 2(\lambda_A - \lambda_B) m_1 m_2 \right)^2 + \frac{1}{2} \mu_0 M_S^2 (N_{11} m_1^2 + N_{22} m_2^2 + N_{33} m_3^2). \tag{5}$$

The stable magnetization state under a certain strain condition can thus be found by minimizing the corresponding free energy density. For illustration, the calculations were performed for the magnetic thin films of cubic (001) $Fe_{81.3}Ga_{18.7}$ (FeGa), $CoFe_2O_4$ (CFO), Ni, and hexagonal (0001) Co, where corresponding materials parameters are listed in Ref. 3, 6 and 14–18.

First, we investigate the influence of normal strain $\varepsilon_{11}$ and $\varepsilon_{22}$ on the magnetization state by assuming $\varepsilon_{12} = 0$. As the first example, Figure 1(a) shows the three-dimensional free energy profiles for the cubic (001) FeGa film under various normal strain conditions, and their in-plane projections ($\theta = 90°$) are shown by the polar plots in Fig. 1(b). The film

dimension is taken as small as $60 \times 60 \times 10$ nm³ to ensure a single-domain configuration.[11] As seen, multiple energy minima and hence the magnetic easy axes appear along the principal $[100]/[\bar{1}00]$ and $[010]/[0\bar{1}0]$ axes under zero strain, clearly illustrating a four-fold cubic symmetry [Fig. 1(b)]. However, it would transform into a two-fold tetragonal symmetry upon anisotropic biaxial in-plane strains, e.g., $(\varepsilon_{11}, \varepsilon_{22}) = (1\%, -1\%)$ and $(-1\%, 1\%)$, where the magnetic easy axes align along the $[100]/[\bar{1}00]$ and $[010]/[0\bar{1}0]$ axes, respectively. Particularly, the easy axes can stabilize at the out-of-plane $[001]/[00\bar{1}]$ axis after applying a negative isotropic biaxial in-plane strain of $(-1\%, -1\%)$ regarding its positive magnetostriction coefficient $\lambda_{100}$,[14] as demonstrated
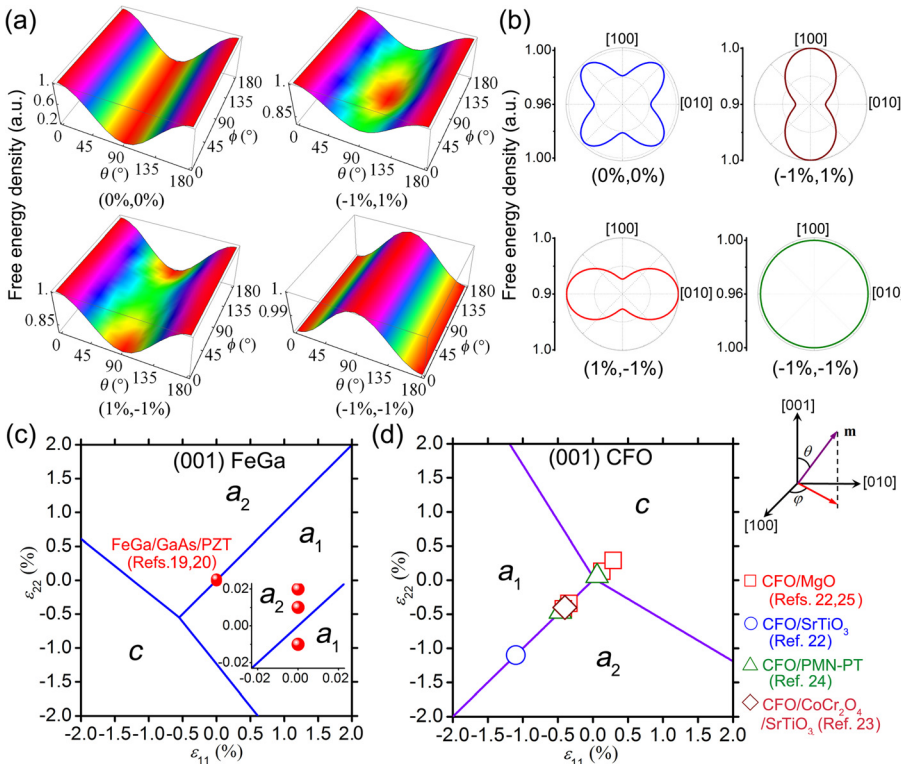


FIG. 1. (a) Profiles of the free energy density of (001) cubic FeGa thin films under various normal strain conditions where $\theta$ and $\varphi$ are the azimuth angles and (b) their corresponding polar plots in the (001) plane. Normal-normal strain-domain structural diagram of (c) (001) cubic FeGa and (d) CFO thin films. Domain definitions and corresponding magnetization components: $a_1$ ($m_1 \neq 0$ and $m_2 = m_3 = 0$), $a_2$ ($m_2 \neq 0$ and $m_1 = m_3 = 0$), and $c$ ($m_3 \neq 0$ and $m_1 = m_2 = 0$); $O_{12}$ ($m_1 \neq 0$, $m_2 \neq 0$ and $m_3 = 0$), $O_{13}$ ($m_1 \neq 0$, $m_3 \neq 0$ and $m_2 = 0$), and $O_{23}$ ($m_2 \neq 0$, $m_3 \neq 0$ and $m_1 = 0$) The film sizes are taken as $60 \times 60 \times 10$ nm³. The solid dots in (c) and open symbols in (d) indicate the experimental results.

by the energy minima at $\theta = 0°$ and $180°$ [Fig. 1(a)] as well as the isotropic in-plane polar plot [Fig. 1(b)].

By further searching the free energy minima by varying both $\varepsilon_{11}$ and $\varepsilon_{22}$ from $-2\%$ to $2\%$, a *normal* strain-domain structural diagram is constructed for such FeGa film [Fig. 1(c)]. The diagram shows the *stable* domain states under a specific strain condition during the magnetic thin film growth. As seen, three tetragonal domains $a_1$, $a_2$, and $c$ (with only one non-zero magnetization component) are exhibited without intermediated states between every two of them, owing to the positive magnetocrystalline coefficient $K_1$ that keeps the energy minima along the principal $\langle 100 \rangle$ cubic axes [Fig. 1(b)]. Furthermore, the domain states can be switched, for example, between $[100]/[\bar{1}00]$ ($a_1$) and $[010]/[0\bar{1}0]$ ($a_2$), by applying a negative and positive anisotropic biaxial in-plane strain of $(0, -0.01\%)$ and $(0,0,0.01\%)$ via piezostrains,[19] respectively. The available experimental results in continuous FeGa thin films are indicated by solid dots in Fig. 1(c). Particularly, such a piezostrain-induced $a_1$ to $a_2$ (and vice versa) switching was experimentally shown to be bistable,[20] i.e., the domain state remains stable even after the applied strain is removed. It is due to the potential barrier from the magnetocrystalline energy[21] between the in-plane $a_1$ and $a_2$ domains. Moreover, an out-of-plane $c$ domain state can be stable in the FeGa thin film, providing the strain is large enough to overcome both the magnetocrystalline and out-of-plane demagnetization energy, e.g., the isotropic biaxial in-plane strain of $(-0.55\%, -0.55\%)$ [Fig. 1(c)].

In comparison to the soft thin-film magnet FeGa with large $M_s$ and relatively low magnetocrystalline coefficient $K_1$, the $c$ domain configuration and the out-of-plane

switching in the hard thin-film magnet CFO would be easier to realize wherein the critical strain is reduced to $(0.03\%, 0.03\%)$ [Fig. 1(d)], mainly due to its much smaller $M_s$ and the larger negative magnetostriction coefficient. As shown in Fig. 1(d), there are also no intermediated domain states in CFO thin films with a positive $K_1$. Furthermore, the calculations agree well with the experimental results in continuous CFO thin films [see those symbols in Fig. 1(d)], wherein the isotropic in-plane biaxial strains can be tuned by varying the underlying substrate,[22–24] film thickness,[23,25] growth temperature,[26] and/or applying a voltage bias to the active piezoelectric substrate like PMN-PT.[24]

Similarly, a normal strain-domain structural diagram for (001) cubic Ni thin film can also be constructed as shown in Fig. 2(a). Differently from the cases in (001) FeGa and CFO films, strain-stabilized three orthorhombic domains $O_{12}$, $O_{13}$, $O_{23}$, and one rhombohedral domain $r$ (with two non-zero and all three non-zero magnetization components, respectively) are exhibited, distributing within the intermediate regions of the tetragonal $a_1$, $a_2$, and $c$ domains. This is mainly due to the *negative* $K_1$ of the Ni film which makes the energy minima shift continuously among the $\langle 001 \rangle$ cubic axes, as directly illustrated by their corresponding polar plots in the (001), (010), (100), and $(1\bar{1}0)/(110)$ planes [Fig. 2(b)], respectively. As seen, the orthorhombic domains $O_{12}$, $O_{13}$, $O_{23}$ exhibit four-fold easy axes (along the $\langle 110 \rangle$ axes) while the rhombohedral domain $r$ presents an eight-fold easy axis (along the $\langle 111 \rangle$ axes).

For clear illustration of the features of easy axis variation within these intermediated domain states, the free energy formalism of the cubic magnets in the (001) plane can be expressed by taking $m_3 = 0$ in Eq. (4), i.e.,

$$f^{\text{cubic}}(\mathbf{m}, \boldsymbol{\varepsilon}) = \left( K_1 + \frac{3\lambda_{100}(c_{11} - c_{12})(\varepsilon_{22} - \varepsilon_{11} - 3/2\lambda_{100})}{2} + \frac{9c_{44}\lambda_{111}^2}{2} \right) m_1^2$$
$$+ \left( -K_1 + \frac{9(c_{11} - c_{12})\lambda_{100}^2}{4} - \frac{9c_{44}\lambda_{111}^2}{2} \right) m_1^4 \pm 6c_{44}\varepsilon_{12}\lambda_{111}m_1\sqrt{1 - m_1^2}, \quad (6)$$

where the terms independent of the magnetization vectors $\mathbf{m}$ were neglected. The feature of corresponding in-plane magnetic easy axis reorientation (e.g., from $a_1$ to $a_2$) would thus depends on the sign of the quartic coefficient (or simply $-K_1$) which is positive for (001) Ni ($\sim 5.138$ kJ/m$^3$), indicating a continuous rotation of the magnetic easy axis (i.e., a *second-order* thermodynamic phase transformation[6]). While for the (001) FeGa and CFO discussed above, negative quartic coefficients of $-13.73$ kJ/m$^3$ and $-117.78$ kJ/m$^3$ are exhibited, respectively, resulting in an abrupt magnetic easy axis reorientation between $a_2$ and $a_1$ (i.e., a *first-order* thermodynamic phase transformation[6]). Free energy formalisms in the (010), (100), and $(1\bar{1}0)/(110)$ planes can similarly be described by taking $m_2 = 0$, $m_1 = 0$, and $m_1 = m_2(-m_2)$, respectively, which would elucidate the corresponding out-of-plane switching features, either abrupt (FeGa, CFO) or continuous (Ni).

The normal strain-domain structural diagram is also calculated for hexagonal magnetic thin film such as (0001) Co

[Fig. 2(c)] by minimizing the corresponding free energy formalism [Eq. (5)] under various normal strains. Different from the cases in (001) cubic thin-film magnets, the magnetic easy axes rotate abruptly in the (001) plane between $a_1$ and $a_2$, while continuously perpendicular to the (001) plane with intermediated $O_{13}$ and $O_{23}$ domains corresponding to the $a_1$-$c$ and $a_2$-$c$ switching, respectively. Also note that both the $O_{13}$ and $O_{23}$ domains occupy larger regions in the diagram, i.e., easier to be stabilized by normal strains, than their counterparts in (001) Ni [Fig. 2(a)], due to the larger strain-independent quartic coefficient of their corresponding free energy formalisms in the (010) and (100) planes, respectively (not shown here).

Now turn to discuss the influence of the in-plane shear strain $\varepsilon_{12}$ on the domain structure (or easy axis orientation) in magnetic thin films. Such in-plane shear strain may exist, for example, in (001) cubic thin-film magnet grown on a (001) tetragonal substrate[27] with $[110] \| [100]_s$ and $[\bar{1}10] \|$
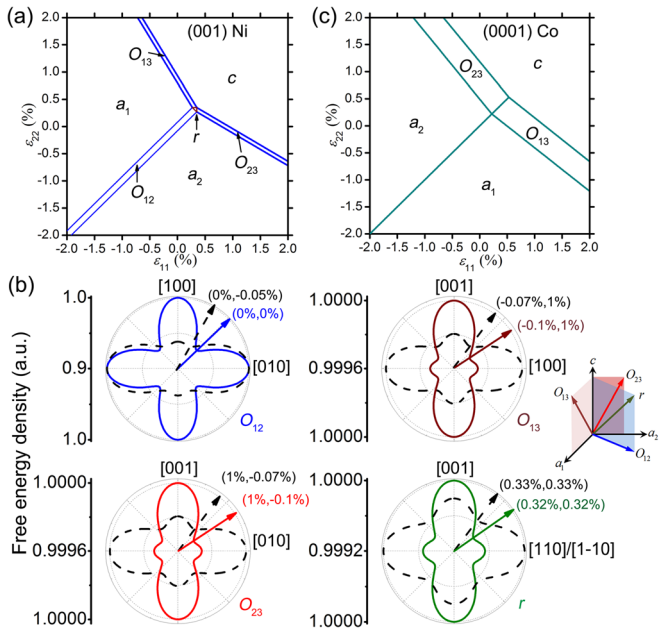
FIG. 2. Normal-normal strain-domain structural diagram of (a) (001) cubic Ni and (c) (0001) hexagonal Co thin films. (b) Polar plots of the free energy density in the (001), (010), (100), and (1–10)/(110) planes of (001) Ni thin films, respectively, indicating the continuous rotation of magnetic easy axes upon various normal strains in the $O_{12}$, $O_{13}$, $O_{23}$, and $r$ ($m_1 \neq 0$, $m_2 \neq 0$ and $m_3 \neq 0$) domain regions, respectively. The arrows denote the easy axis orientations in one quadrant.

$[010]_s$, or by operating an adjacent piezoelectric actuator in shear mode.[28] Figure 3(a) shows the *shear-normal* strain-domain structural diagram for the (001) Ni film, where an in-plane shear strain $\varepsilon_{12}$ (−1%–1%) is imposed with biaxial in-plane isotropic normal strains ($\varepsilon_{11} = \varepsilon_{22}$). Compared to the case with zero shear strain [Fig. 2(a)], the orthorhombic $O_{12}$ domains take up a much larger region, and with reduced two-fold (uniaxial) symmetry for the magnetic easy axes, i.e., along the $[110]/[\bar{1}\bar{1}0]$ directions ($O_{12}^\alpha$) and the $[1\bar{1}0]/[\bar{1}10]$ directions ($O_{12}^\beta$) corresponding to compressive and tensile $\varepsilon_{12}$, respectively, as directly illustrated by the polar plots of free energy density in the (001) plane [the first row in Fig. 3(b)]. Similarly, a reduced four-fold magnetic

easy axis is exhibited for the rhombohedral domains $r^\alpha$ and $r^\beta$, indicating easy axes along the $[111]/[\bar{1}\bar{1}\bar{1}]$ or $[1\bar{1}1]/[\bar{1}1\bar{1}]$ directions, respectively. Such easy axis alignments are further illustrated by the polar plots of free energy density on the $(1\bar{1}0)$, and (110) planes, respectively [the second row in Fig. 3(b)]. The (0001) hexagonal Co thin film shows a similar shear-normal strain-domain structural diagram, but with larger area fractions for the rhombohedral $r^\alpha$ and $r^\beta$ domains [Fig. 3(c)] than those in cubic Ni [Fig. 3(a)].

Furthermore, the obtained domain states can possibly undergo thermal excitations[29] even at room temperature, particularly for those at/near the phase boundary where the potential barriers $h$ separating different phases are comparable to $k_B T$ ($k_B$ denotes the Boltzmann constant and $T$ the Kelvin temperature). As shown in Fig. 4(a), the rhombohedral domain $r$ in the (001) Ni film ($\varepsilon_{11} = \varepsilon_{22} = 0.33\%$ and $\varepsilon_{12} = 0$) would readily transform to other domain states upon thermal fluctuations, mainly due to the low potential barrier $h$. Regarding an established criterion of $h > 60k_B T$ for a *thermally* stable magnetization state,[30] we further calculate the room-temperature ($T = 298$ K) normal-normal and shear-normal strain-domain stability diagrams of (001) Ni [see Figs. 4(b) and 4(c), respectively] as an example by taking $h = \Delta f_{min} \times V$, where $\Delta f_{min}$ is the minimum energy difference between the given domain state and other possible ones and $V$ the volume of the thin-film magnet. As illustrated, most strain-stabilized domain states remain thermally stable, i.e., with a stability factor of $h/k_B T$ higher than 60, even at a small dimension of $60 \times 60 \times 10$ nm$^3$, except those in the vicinity of the phase boundaries. But all the intermediated domain states, e.g., the $O_{13}$, $O_{12}$, $O_{23}$ in Fig. 4(b) and $r^\alpha$, $r^\beta$ in Fig. 4(c), are thermally unstable at the present size. The area fraction of these unstable regions (with $h \leq 60k_B T$, approximately colored in violet) $f_u$ can be reduced by increasing the magnetostriction coefficient $\lambda_{100}$ but is almost independent on $\lambda_{111}$ in such (001) cubic magnetic thin films upon zero in-plane shear strain $\varepsilon_{12}$, whereas both $\lambda_{100}$ and $\lambda_{111}$ have a significant influence on $f_u$ upon a non-zero $\varepsilon_{12}$ [Fig. 4(d)]. This indicates that $\varepsilon_{12}$ affects the domain structure and stability only based on $\lambda_{111}$, as also indicated by Eq. (6).
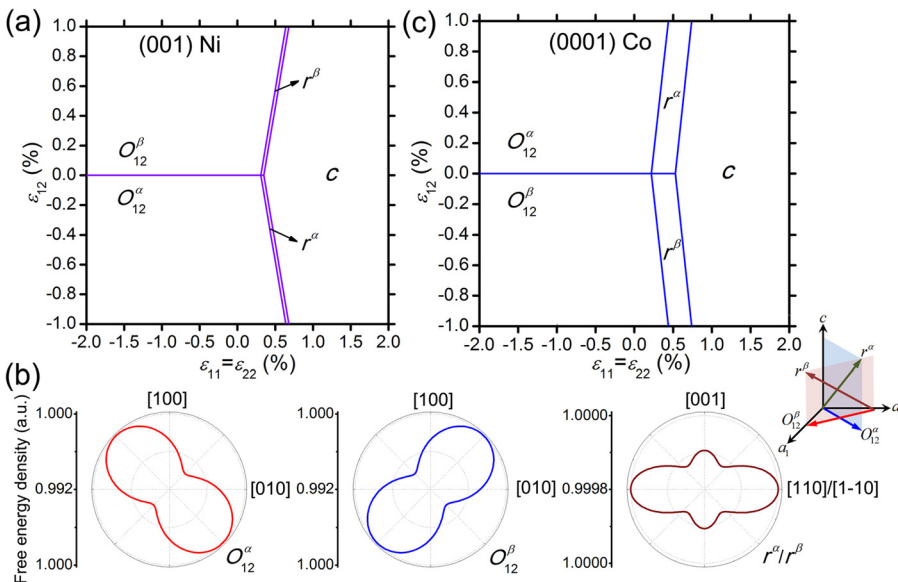


FIG. 3. Shear-normal strain-domain structural diagram of (a) (001) cubic Ni and (c) (0001) hexagonal Co thin films. (b) Polar plots of the free energy density in the (001) plane to illustrate the $O_{12}^\alpha$ and $O_{12}^\beta$ domains, and in the (1–10)/(110) planes for the $r^\alpha/r^\beta$ domains. The arrows denote the easy axis orientation in one quadrant.
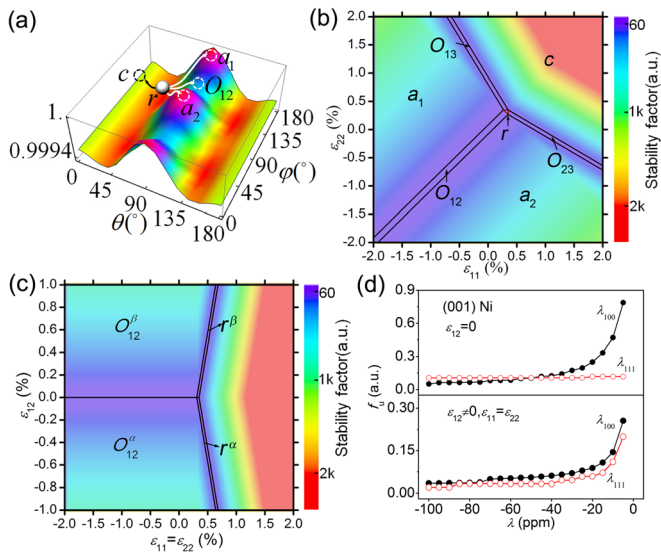
FIG. 4. (a) Free energy density profile of the (001) Ni thin film of $60 \times 60 \times 10$ nm$^3$ in a rhombohedral $r$ domain ($\varepsilon_{11} = \varepsilon_{22} = 0.33\%$, $\varepsilon_{12} = 0$). The corresponding (b) normal-normal and (c) shear-normal strain-domain stability maps of the (001) Ni thin film, with zero and non-zero in-plane shear strain $\varepsilon_{12}$, respectively. The solid lines indicate the phase boundaries without including possible thermal excitations. The color bar denotes the stability factor which essentially should be higher than 60 to ensure a thermally stable domain state. (d) Influences of the magnetostriction constants $\lambda$ (i.e., $\lambda_{100}$ and $\lambda_{111}$) on the area fraction of the unstable region $f_u$ with zero $\varepsilon_{12}$ (the upper panel), and non-zero $\varepsilon_{12}$ (the lower panel). Note that the $\lambda_{111}$ keeps invariant (i.e., $-24.3$ ppm) when investigating the dependence of $\lambda_{100}$, and vice versa.

So far we have studied, using thermodynamic analysis, the strain effects on domain structures and corresponding thermal stability in single-domain magnetic thin films with either the cubic or hexagonal crystal symmetry. Various strain-induced domain states are obtained, including the tetragonal $a_1$, $a_2$, $c$ domains with two-fold easy axes, orthorhombic $O_{12}$, $O_{13}$, $O_{23}$ domains with four-fold easy axes, and the rhombohedral $r$ domain with eight-fold easy axes, which exhibit with one, two, and three non-zero magnetization components, respectively. Among them, the tetragonal domains can be stabilized by reasonable normal strains $\varepsilon_{11}$ and $\varepsilon_{22}$ even at a small size of $60 \times 60 \times 10$ nm$^3$ for the thin film [Fig. 4(b)], while the four-fold $O_{12}$ domain can be reduced to the two-fold $O_{12}^{\alpha}$ and $O_{12}^{\beta}$ domains upon applying an in-plane shear strain and further be stabilized [Fig. 4(c)]. However, the four-fold $O_{13}$ and $O_{23}$, eight-fold $r$ and corresponding four-fold $r^{\alpha}$, $r^{\beta}$ domains are more difficult to become thermally stable, and larger geometric size and/or magnetostriction coefficients are thus required. The obtained results would contribute to both the fundamental understanding of the strain-magnetization correlation in magnetic thin films and the development of strain-engineered magnetic nanostructures for novel functionalities.

[1] A. Hubert and R. Schäfer, *Magnetic domains—The Analysis of Magnetic Microstructures* (Springer-Verlag, Berlin, 2000).

[2] M. T. Johnson, P. J. H. Bloemen, F. J. A. d. Broeder, and J. J. d. Vries, Rep. Prog. Phys. **59**, 1409 (1996).

[3] D. Sander, Rep. Prog. Phys. **62**, 809 (1999).

[4] K. H. Ahn, T. Lookman, and A. R. Bishop, Nature **428**, 401 (2004); A. Mukherjee, W. S. Cole, P. Woodward, M. Randeria, and N. Trivedi, Phys. Rev. Lett. **110**, 157201 (2013); M. Liu, J. Hoffman, J. Wang, J. Zhang, B. Nelson-Cheeseman, and A. Bhattacharya, Sci. Rep. **3**, 1876 (2013).

[5] N. A. Pertsev, Phys. Rev. B **78**, 212102 (2008).

[6] J.-M. Hu and C. W. Nan, Phys. Rev. B **80**, 224416 (2009).

[7] D. G. Schlom, L. Q. Chen, C. B. Eom, K. M. Rabe, S. K. Streiffer, and J. M. Triscone, Annu. Rev. Mater. Res. **37**, 589 (2007).

[8] S. C. Seel, C. V. Thompson, S. J. Hearne, and J. A. Floro, J. Appl. Phys. **88**, 7079 (2000).

[9] W. Eerenstein, M. Wiora, J. L. Prieto, J. F. Scott, and N. D. Mathur, Nature Mater. **6**, 348 (2007).

[10] J.-M. Hu, Z. Li, L.-Q. Chen, and C.-W. Nan, Nat. Commun. **2**, 553 (2011); Adv. Mater. **24**, 2869 (2012).

[11] J.-M. Hu, G. Sheng, J. X. Zhang, C. W. Nan, and L. Q. Chen, Appl. Phys. Lett. **98**, 112505 (2011); J. Appl. Phys. **109**, 123917 (2011).

[12] J.-M. Hu, Z. Li, J. Wang, J. Ma, Y. H. Lin, and C. W. Nan, J. Appl. Phys. **108**, 043909 (2010).

[13] W. P. Mason, Phys. Rev. **82**, 715 (1951).

[14] Cubic Fe$_{81.3}$Ga18.$_7$: $K_1 = 20$ kJ/m$^3$, $K_2 = -45$ kJ/m$^3$, $c_{11} = 196$ GPa, $c_{12} = 156$ GPa, $c_{44} = 123$ GPa; $\lambda_{100} = 264$ ppm, $M_s = 1.43 \times 10^6$ A/m (Ref. 15); Cubic Ni: $K_1 = -5$ kJ/m$^3$, $c_{11} = 246.5$ GPa, $c_{12} = 147.3$ GPa, $c_{44} = 124.7$ GPa, $\lambda_{100} = -45.9$ ppm, $\lambda_{111} = -24.3$ ppm, $M_s = 4.85 \times 10^5$ A/m (Refs. 6, 16, and 18); Cubic CoFe$_2$O$_4$: $K_1 = 200$ kJ/m$^3$, $c_{11} = 286$ GPa, $c_{12} = 173$ GPa, $c_{44} = 97$ GPa, $\lambda_{100} = -590$ ppm, $\lambda_{111} = 120$ ppm, $M_s = 3.5 \times 10^5$ A/m (Refs. 6 and 13); Hexagonal Co: $K_1 = 410$ kJ/m$^3$, $K_2 = 100$ kJ/m$^3$, $c_{11} = 307$ GPa, $c_{12} = 165$ GPa, $c_{44} = 75.5$ GPa; $\lambda_A = -45$ ppm, $\lambda_B = -95$ ppm, $M_s = 1.43 \times 10^6$ A/m (Refs. 3, 16–18).

[15] J. X. Zhang and L. Q. Chen, Acta Mater. **53**, 2845 (2005).

[16] R. E. Newnham, *Properties of Materials: Anisotropy, Symmetry, Structure* (OUP, Oxford, 2005).

[17] R. Bozorth, Phys. Rev. **96**, 311 (1954).

[18] W. Gong, H. Li, Z. Zhao, and J. Chen, J. Appl. Phys. **69**, 5119 (1991).

[19] D. E. Parkes, S. A. Cavill, A. T. Hindmarch, P. Wadley, F. McGee, C. R. Staddon, K. W. Edmonds, R. P. Campion, B. L. Gallagher, and A. W. Rushforth, Appl. Phys. Lett. **101**, 072402 (2012).

[20] S. A. Cavill, D. E. Parkes, J. Miguel, S. S. Dhesi, K. W. Edmonds, R. P. Campion, A. W. Rushforth, Appl. Phys. Lett. **102**, 032405 (2013).

[21] J.-M. Hu, Z. Li, J. Wang, and C. W. Nan, J. Appl. Phys. **107**, 093912 (2010).

[22] T. Dhakal, D. Mukherjee, R. Hyde, P. Mukherjee, M. H. Phan, H. Srikanth, and S. Witanachchi, J. Appl. Phys. **107**, 053914 (2010).

[23] Y. Suzuki, G. Hu, R. B. van Dover, and R. J. Cava, J. Magn. Magn. Mater. **191**, 1 (1999).

[24] J.-Y. Kim, L. Yao, and S. van Dijken, J. Phys: Condens. Matter **25**, 082205 (2013).

[25] A. Lisfi, C. M. Williams, L. T. Nguyen, J. C. Lodder, A. Coleman, H. Corcoran, A. Johnson, P. Chang, A. Kumar, and W. Morgan, Phys. Rev. B **76**, 054405 (2007).

[26] P. C. Dorsey, P. Lubitz, D. B. Chrisey, and J. S. Horwitz, J. Appl. Phys. **79**, 6338 (1996).

[27] T. H. E. Lahtinen, Y. Shirahata, L. Yao, K. J. A. Franke, G. Venkataiah, T. Taniyama, and S. van Dijken, Appl. Phys. Lett. **101**, 262405 (2012).

[28] H. Boukari, C. Cavaco, W. Eyckmans, L. Lagae, and G. Borghs, J. Appl. Phys. **101**, 054903 (2007); N. Moutis, D. Suarez-Sandoval, and D. Niarchos, J. Magn. Magn. Mater. **320**, 1050 (2008); L. Thevenard, J. Y. Duquesne, E. Peronne, H. J. von Bardeleben, H. Jaffres, S. Ruttala, J. M. George, A. Lemaître, and C. Gourdon, Phys. Rev. B **87**, 144402 (2013).

[29] J. G. Zhu, Proc. IEEE **96**, 1786 (2008).

[30] R. F. L. Evans, R. W. Chantrell, U. Nowak, A. Lyberatos, and H. J. Richter, Appl. Phys. Lett. **100**, 102402 (2012).